Sum rules and missing spectral weight in magnetic neutron scattering in the cuprates

J. Lorenzana
SMC-INFM, ISC-CNR, Dipartimento di Fisica, Università di Roma "La Sapienza", P. Aldo Moro 2, 00185 Roma, Italy

G. Seibold
Institut für Physik, BTU Cottbus, P. O. Box 101344, 03013 Cottbus, Germany

R. Coldea
Oxford Physics, Clarendon Laboratory, Oxford OX1 3PU, United Kingdom
(Received 5 July 2005; published 15 December 2005)

We present estimates in the Hubbard and Heisenberg models for the spectral weight in magnetic neutron-scattering experiments on the cuprates. With the aid of spin-wave theory and the time-dependent Gutzwiller approximation, we discuss how the spectral weight is distributed among the different channels and between high and low energies. In addition to the well known total moment sum rule, we discuss sum rules for each component of the dynamical structure factor tensor which are peculiar for spin-$\frac{1}{2}$ systems. The various factors that reduce the spectral weight at the relevant energies are singled out and analyzed, such as shielding factors, weight at electronic energies, multimagnon process, etc. Although about 10–15 % of the naively expected weight is detected in experiments, after consideration of these factors the missing weight is within the experimental uncertainties. A large fraction of the spectral weight is hard to detect with present experimental conditions.

DOI: 10.1103/PhysRevB.72.224511 PACS number(s): 74.25.Ha, 78.70.Nx, 71.10.Fd, 74.72.−h

I. INTRODUCTION

Magnetic neutron scattering (MNS) in high-temperature superconducting cuprates usually detects about 10–15 % of the spectral weight dictated by a naive application of sum rules. For example, the total weight in a wide range of energy and momentum in a recent experiment[1] in $La_{2-x}Ba_xCuO_4$, with $x=0.125$, is $\sim 0.22\mu_B^2$, whereas in the insulating phase the naive expectation from sum rules is that one should find $2\mu_B^2$. It is usually argued that this value should be corrected for the hole destruction of moments by a $1-x$ factor, which still leaves a large fraction of spectral weight undetected.

This raises various problems in the interpretation of MNS. For example, it has been argued that the average of the dynamical susceptibility weighted by the Fourier transform of the magnetic interaction can be used to estimate the energy involved in magnetic pairing and its temperature dependence.[2–6] Clearly, to obtain an absolute estimate the spectral weight problem needs to be sorted out first. Furthermore, modeling the dynamical structure factor probed by MNS becomes rather problematic since sensible theoretical models do satisfy sum rules. Indeed, any theoretical claim of intensity agreement with the measured dynamical structure factor in absolute units needs to explain how the sum rule is satisfied or why it is violated. This is even more stringent in spin-only models for which neither $1-x$ factors nor shielding corrections apply.

The purpose of this work is to explain this apparent discrepancy. We provide theoretical estimates of the various factors that correct the sum rule and estimate what fraction of the spectral weight is accessible to present-day experimental conditions. Theoretical estimates are performed in the antiferromagnetic (AFM) phase using the Heisenberg and the Hubbard model combining spin-wave theory, numerical results, and the time-dependent Gutzwiller approximation (TDGA),[7–9] and in the doped phase in the Hubbard model within the TDGA. Apart from the mentioned $1-x$ factor, we discuss the so called "shielding factors" due to an incomplete formation of magnetic moments. We estimate the spectral weight loss to electronic transitions at energies too high to be detectable by present-day inelastic magnetic neutron-scattering experiments and also the weight in multimagnon processes, which is either at too high energies or is so broad in energy and momentum that it is not detectable in unpolarized neutron-scattering experiments. After consideration of all these factors, we arrive at the conclusion that within the experimental uncertainties the sum rule is not violated (which is reassuring), on the other hand a major fraction of the spectral weight is very hard to detect with present experimental conditions.

The outline of the paper is as follows. In Sec. II, we briefly review the theory of magnetic neutron scattering and the relevant sum rules to fix notations. This section also has a pedagogical character. Apart from the well known total moment sum rule, we discuss sum rules for each component of the dynamical structure factor tensor which, to the best of our knowledge, have not been applied in the present context. We also highlight some simple experimental facts that are usually assumed as granted in experimental works, such as domain averages (Sec. II C), but are often overlooked in theoretical works. In Sec. III, we discuss the spectral weight distribution in the undoped case and in Sec. IV we discuss the doped case. We conclude in Sec. V.

II. MAGNETIC NEUTRON SCATTERING

We start with a short review of magnetic neutron scattering to fix notations and discuss the sum rules that are relevant to our problem.

The magnetic neutron-scattering cross section is given by[10]

$$\frac{d^2\sigma}{d\Omega\, dE'} = N\frac{k'}{k}\left(\frac{\gamma r_e}{2\mu_B}\right)^2 |F(\boldsymbol{q})|^2 e^{-2W(\boldsymbol{q})} \times \sum_{\alpha\beta} (\delta_{\alpha\beta} - \hat{q}_\alpha \hat{q}_\beta) S^{\alpha\beta}(\boldsymbol{q},\omega), \quad (1)$$

where $e^{-2W(q)}$ is the Debye-Waller factor, $\boldsymbol{q} \equiv \boldsymbol{k} - \boldsymbol{k}'$ ($\hat{\boldsymbol{q}} \equiv \mathbf{q}/|\boldsymbol{q}|$), $\boldsymbol{k}$ ($\boldsymbol{k}'$) is the initial (final) wave vector of neutrons, and $(\gamma r_e/2\mu_B)^2 = 72.65 \times 10^{-3}$ barn$/\mu_B^2$. The magnetic form factor is given by $F(\boldsymbol{q}) = \int dr\, e^{i\boldsymbol{q}\cdot\boldsymbol{r}} |\phi(\boldsymbol{r})|^2$, where $\phi(\boldsymbol{r})$ is a Wannier orbital and we defined the dynamical structure factor tensor,

$$S^{\alpha\beta}(\boldsymbol{q},\omega) = \frac{(g\mu_B)^2}{NZ}\sum_{\mu\nu} e^{-\beta E_\mu} \langle\mu|S^\alpha_{-\boldsymbol{q}}|\nu\rangle\langle\nu|S^\beta_{\boldsymbol{q}}|\mu\rangle \times \delta(\hbar\omega - E_\nu + E_\mu), \quad (2)$$

where g is the Landé g factor. For free electrons $g = 2.0023$. In a solid a different value may be appropriate, which may also depend on direction. For example, Ref. 11 quotes $g = 2.08$ in the plane and $g = 2.36$ perpendicular to the plane for a typical cuprate. For simplicity, we take an isotropic g unless otherwise specified. $S^\alpha_{\boldsymbol{q}}$ is the Fourier transform of the α component of the spin operator and Z is the partition function. The dynamical structure factor $S^{\alpha\beta}(\boldsymbol{q},\omega)$ obeys detailed balance $S^{\alpha\beta}(\boldsymbol{q},\omega) = e^{\beta\hbar\omega} S^{\alpha\beta}(-\boldsymbol{q},-\omega)$.

A. Sum rules

We will discuss sum rules for effective models of the magnetic dynamics. Because effective models restrict the Hilbert space, sum rules turn out to be model-dependent and therefore should be applied with care on modeling a real system, as discussed below. Our considerations are based on the two most popular models in this context, namely the Heisenberg and the Hubbard model, respectively.

The so called total moment sum rule is usually formulated within a Heisenberg model with spin S and reads

$$M_0 \equiv \frac{1}{N}\sum_{\boldsymbol{q}\alpha}\int_{-\infty}^{\infty} d(\hbar\omega) S^{\alpha\alpha}(\boldsymbol{q},\omega) = (g\mu_B)^2 S(S+1). \quad (3)$$

This applies to a system where magnetic ions have one or several partially filled orbitals (for example, a rare earth ion with a partially filled f shell) and well formed magnetic moments, i.e., when double occupancy of a given orbital is negligible.

Within this work, we will restrict ourselves to systems where ions have only one partially filled orbital and the system can be modeled with a one-band Hubbard model,

$$H = -t\sum_{\langle ij\rangle\sigma} c^\dagger_{i\sigma} c_{j\sigma} - t'\sum_{\langle\langle ij\rangle\rangle\sigma} c^\dagger_{i\sigma} c_{j\sigma} + U\sum_i n_{i\uparrow} n_{i\downarrow}. \quad (4)$$

Here $c^\dagger_{i\sigma}$ ($c_{i\sigma}$) destroys (creates) an electron with spin σ at site i, and $n_{i\sigma} = c^\dagger_{i\sigma} c_{i\sigma}$. U is the on-site Hubbard repulsion and both nearest- ($\sim t$) and next-nearest- ($\sim t'$) neighbor hopping has been included. Most of our considerations apply also to other models where ions have only one partially filled orbital per atom, such as the usual three-band Hubbard model for cuprates with Cu d and O p orbitals.

We define for later use the spin autocorrelation function and the zeroth moment of the diagonal components of the dynamical structure factor as

$$S^{\alpha\alpha}(\omega) \equiv \frac{1}{N}\sum_{\boldsymbol{q}} S^{\alpha\alpha}(\boldsymbol{q},\omega) \quad (5)$$

$$M_0^\alpha \equiv \int_{-\infty}^{\infty} d(\hbar\omega) S^{\alpha\alpha}(\omega). \quad (6)$$

When one has one orbital per site (i.e., a spin-$\frac{1}{2}$ system), more stringent sum rules than Eq. (3) apply. Indeed *each component* of the dynamical structure factor satisfies a separate sum rule. For example, from Eqs. (2), (5), and (6) one finds

$$M_0^z = \frac{(g\mu_B)^2}{N^2 Z}\sum_{\mu\boldsymbol{q}} e^{-\beta E_\mu}\langle\mu|S^z_{-\boldsymbol{q}} S^z_{\boldsymbol{q}}|\mu\rangle = \frac{(g\mu_B)^2}{4}(n - 2D), \quad (7)$$

where $S^z_{\boldsymbol{q}} = \Sigma_i e^{-i\boldsymbol{q}\cdot\boldsymbol{r}_i} S^z_i$ with $S^z_i = (n_{i\uparrow} - n_{i\downarrow})/2$ and we used that $n^2_{i\sigma} = n_{i\sigma}$. We also defined the thermal ($\langle\cdots\rangle$) and spacial averages of the orbital occupancy,

$$n \equiv \frac{1}{N}\sum_{i\sigma}\langle n_{i\sigma}\rangle,$$

and double occupancy,

$$D \equiv \frac{1}{N}\sum_i \langle n_{i\uparrow} n_{i\downarrow}\rangle.$$

Analogous proofs hold for the other components,

$$M_0^\alpha = \mu_B^2(n - 2D), \quad (8)$$

where we took $g = 2$. (We will occasionally restore g below when convenient for clarity.) Equation (8) also follows from the fact that the quantization axis in Eq. (7) is arbitrary.

Equation (3) is valid in the Heisenberg model where $D = 0$ and S is arbitrary. Equation (8) in contrast is valid for $S = 1/2$ systems but without restriction in D.

The factor $(n - 2D)$ in Eq. (8) is the probability to find an atom singly occupied and reflects the fact that doubly occupied or empty atoms do not produce magnetic scattering of neutrons reducing the total scattering cross section. This is sometimes called the "shielding factor."

One can also prove that the total weight of the off-diagonal components of $S^{\alpha\beta}$ adds to zero. First notice that only the symmetric part of $S^{\alpha\beta}$ contributes to Eq. (1),

$$\sum_{\alpha\beta}(\delta_{\alpha\beta}-\hat{q}_\alpha\hat{q}_\beta)S^{\alpha\beta}(\boldsymbol{q},\omega)$$

$$=\frac{1}{2}\sum_{\alpha\beta}(\delta_{\alpha\beta}-\hat{q}_\alpha\hat{q}_\beta)[S^{\alpha\beta}(\boldsymbol{q},\omega)+S^{\beta\alpha}(\boldsymbol{q},\omega)].$$

Using the Lehmann representation Eq. (2), one can show that

$$M_0^{\alpha\beta}\equiv\frac{1}{2N}\sum_q\int_{-\infty}^{\infty}d(\hbar\omega)[S^{\alpha\beta}(\boldsymbol{q},\omega)+S^{\beta\alpha}(\boldsymbol{q},\omega)]$$

$$=\delta_{\alpha\beta}\mu_B^2(n-2D), \tag{9}$$

which gives us a sum rule for each component of $S^{\alpha\beta}(q,\omega)$.

We are not aware of references quoting the sum rule Eq. (9), although the result is so simple that we doubt it is original.

If $S^z_{\rm tot}=\Sigma_i S^z_i$ is a good quantum number, $S^{\alpha\beta}(q,\omega)$ becomes diagonal with $S^{xx}(q,\omega)=S^{yy}(q,\omega)$.[10] In this case, we can write the cross section as

$$\frac{d^2\sigma}{d\Omega\,dE'}=N\frac{k'}{k}\left(\frac{\gamma r_e}{2\mu_B}\right)^2|F(\boldsymbol{q})|^2e^{-2W(\boldsymbol{q})}$$

$$\times[(1-\hat{q}_z^2)S^{zz}(\boldsymbol{q},\omega)+(1+\hat{q}_z^2)S^{xx}(\boldsymbol{q},\omega)]. \tag{10}$$

We will restrict ourselves to systems where this expression applies.

B. Ordered states and Bragg scattering

In the presence of long-range magnetic order, the system shows magnetic elastic scattering. We will consider phases in which spin rotational invariance is broken with order along the z axis (i.e., stripes, AFM, etc.). We assume a magnetic unit cell with N_a^M atoms ($N_a^M=2$ for the AFM state at half-filling) at positions $\boldsymbol{R}+\boldsymbol{\delta}_i$, with $\boldsymbol{R}$ the cell position and $\boldsymbol{\delta}_i$ the position of the atoms within the cell ($i=1,\ldots,N_a^M$). The vectors $\boldsymbol{R}$ form a Bravais lattice. For such a magnetic structure, we have

$$\langle S^z_{\boldsymbol{q}}\rangle=N\sum_{\boldsymbol{Q}_M}\delta_{\boldsymbol{q}-\boldsymbol{Q}_M}m_{\boldsymbol{Q}_M},$$

where the sum is over the magnetic reciprocal basis vectors and we defined

$$m_{\boldsymbol{Q}_M}\equiv\frac{1}{N_a^M}\sum_i^{N_a^M}e^{i\boldsymbol{Q}_M\cdot\boldsymbol{\delta}_i}m_i, \tag{11}$$

and the local site-dependent magnetization $m_i=\langle n_{i\uparrow}-n_{i\downarrow}\rangle/2$.

It is convenient to define the fluctuation operator,

$$\delta S^z_q\equiv S^z_q-\langle S^z_q\rangle.$$

With these definitions, the longitudinal structure factor can be set as

$$S^{zz}(\boldsymbol{q},\omega)=(g\mu_B)^2\Bigg[N\sum_{\boldsymbol{Q}_M}m^2_{\boldsymbol{Q}_M}\delta(\boldsymbol{q}-\boldsymbol{Q}_M)\delta(\hbar\omega)$$

$$+\sum_\nu|\langle 0|\delta S_{\boldsymbol{q}}|\nu\rangle|^2\delta(\hbar\omega-E_\nu+E_0)\Bigg], \tag{12}$$

where for simplicity we set $T=0$ and $\delta(\boldsymbol{q})$ is Kronecker's δ whereas $\delta(\hbar\omega)$ is Dirac's δ. The first term in the brackets describes Bragg peaks. The weight of the peaks is given by the square of the Fourier transform of the magnetization inside the magnetic unit cell Eq. (11). The second term describes inelastic scattering. The inelastic part (only) of the dynamical structure factor is related to the dynamical susceptibility via the fluctuation dissipation theorem.

C. Domain average

For the case discussed above of a diagonal structure factor tensor, the cross section involves the factors $(1-\hat{q}_\alpha^2)$. These are polarization factors for scattering with unpolarized neutrons and are rooted in the dipolar interaction between neutrons and the electron spin. In experimental works, often the polarization factors $(1-\hat{q}_\alpha^2)$ are included in the definition of the dynamical structure factor and an average over the orientation of domains, $\langle\cdots\rangle_{\rm dom}$, is done,

$$S^{\rm eff}(\boldsymbol{q},\omega)=\sum_\alpha\langle(1-\hat{q}_\alpha^2)\rangle_{\rm dom}S^{\alpha\alpha}(\boldsymbol{q},\omega). \tag{13}$$

For a paramagnet, all directions are equivalent, $S^{\alpha\alpha}(\boldsymbol{q},\omega)$ does not depend on α, and $\langle(1-\hat{q}_\alpha^2)\rangle_{\rm dom}=\frac{2}{3}$. Ordered systems will be characterized by an order parameter that is a vector like the staggered magnetization. In general, a real sample will consist of domains with different orientations of the order parameter. For a distribution of orientations that is completely isotropic in spin space, $\langle(1-\hat{q}_\alpha^2)\rangle_{\rm dom}=\frac{2}{3}$.

Consider now scattering from a quasi-two-dimensional (2D) system with the c direction defined perpendicular to the plane and the a and b directions in the plane. In quasi-2D systems, the most common experimental configuration is that the planes are perpendicular to the incident neutron beam, and, depending on the energy, the component of $\boldsymbol{q}$ perpendicular to the plane, $\boldsymbol{q}_c$ may be larger than the components in the plane. In the extreme case that $\hat{q}_c\gg\hat{q}_a,\hat{q}_b$, one can put [cf. Eq. (13)]

$$S^{\rm eff}(\boldsymbol{q},\omega)=S^{aa}(\boldsymbol{q},\omega)+S^{bb}(\boldsymbol{q},\omega). \tag{14}$$

This is valid regardless of the domain distribution. In order to evaluate this expression, it is convenient to use a domain-dependent reference system in which the z axis follows the ordered moment of the domain. In the case of an *isotropic* distribution of domains, one recovers $\langle(1-\hat{q}_\alpha^2)\rangle_{\rm dom}=\frac{2}{3}$. That is,

$$S^{\rm eff}(\boldsymbol{q},\omega)=\frac{2}{3}[S^{xx}(\boldsymbol{q},\omega)+S^{yy}(\boldsymbol{q},\omega)]+\frac{2}{3}S^{zz}(\boldsymbol{q},\omega), \tag{15}$$

where we have grouped the transverse contribution. On the other hand, one usually deals with systems that have easy planes or easy axes. In cuprates, for example, the ordered moment is usually in the Cu-O plane or close to that plane. For a distribution of the ordered moment which is isotropic *within the plane* and in the above scattering geometry

$$S^{\text{eff}}(\boldsymbol{q},\omega)=\frac{1}{2}[S^{xx}(\boldsymbol{q},\omega)+S^{yy}(\boldsymbol{q},\omega)]+S^{zz}(\boldsymbol{q},\omega). \quad (16)$$

The 1/2 factor is due to the fact that one transverse mode is perpendicular to the plane and becomes silent in this configuration.

For reasons that will be clear below real experiments detect mainly the transverse structure factor. Comparing Eqs. (15) and (16), we see that in order to accurately estimate spectral weights from experiment, precise information is needed on the domain distribution since the transverse component appears with different weight.

The condition $\hat{q}_c \gg \hat{q}_a, \hat{q}_b$ is rather extreme. Instead, in the present scattering geometry, $\hat{q}_c/\hat{q}_a$, $\hat{q}_c/\hat{q}_b$ will gradually decrease as the energy is increased. This will cause the factors weighting the transverse and the longitudinal part to depend on energy. Due to the larger sensibility to the transverse part in a real experiment, this will lead to an apparent loss of spectral weight as the energy increases.

In an ideal experiment where all components are detected with equal sensitivity, one will not see a loss of spectral weight but rather a transfer of spectral weight from the longitudinal to the transverse part as the energy increases. Indeed, $S^{\text{eff}}(\boldsymbol{q},\omega)$ satisfies the sum rule

$$M_0^{\text{eff}} \equiv \frac{1}{N}\sum_{\boldsymbol{q}} \int_{-\infty}^{\infty} d(\hbar\omega) S^{\text{eff}}(\boldsymbol{q},\omega) = 2(n-2D)\mu_B^2, \quad (17)$$

independently of what the distribution of domains or the scattering geometry is.

D. Experimental considerations

On analyzing experimental data, one should take into account that in unpolarized inelastic neutron scattering experiments, magnetic and nonmagnetic scattering cannot be unambiguously identified. In the insulating phase, this problem can be reduced by fitting the data with a simple model such as spin-wave theory. Due to the lack of a simple theory in the doped phase, a similar procedure is not possible. In this case, the usual experimental practice is to report as "magnetic scattering" only those features which satisfy certain criteria such as being reasonably sharp in momentum space and show a "magnetic-like" temperature dependence and form factor dependence across different Brillouin zones. All the rest is assumed to be background of unknown origin. Below, we analyze the distribution of weight in the insulator to get a hint of the distribution of spectral weight in the different channels and where to expect sharp and where to expect broad features.

III. HALF-FILLING

A. Spectral weights in the Heisenberg model

We start by neglecting the shielding factors and estimate the spectral weights in the Heisenberg model within spin-wave theory (SWT). We will show below how to apply these results when shielding factors are important corrections. Since we are interested in gross distributions of spectral weight, for simplicity we consider a Heisenberg model with nearest-neighbor interactions and neglect other terms such as four-ring exchange.

1. Longitudinal part

In order to write the longitudinal dynamical structure factor, we introduce the following notations. For an AFM, the S_i^z operator can be written within SWT as

$$S_i^z = (S-\mathcal{N}_i)e^{-i\boldsymbol{Q}_{\text{AFM}}\cdot\boldsymbol{r}_i},$$

where $\mathcal{N}_i$ is the number operator for Holstein-Primakoff bosons and $\boldsymbol{Q}_{\text{AFM}}=(\pi,\pi)$ taking the lattice constant $a=1$. For the Fourier transform $S_{\boldsymbol{q}}^z=\Sigma_i e^{-i\boldsymbol{q}\cdot\boldsymbol{r}_i}S_i^z$ we have

$$S_{\boldsymbol{q}}^z = NS\delta(\boldsymbol{q}-\boldsymbol{Q}_{\text{AFM}}) - \mathcal{N}_{\boldsymbol{q}-\boldsymbol{Q}_{\text{AFM}}}.$$

It is convenient to write $\mathcal{N}_{\boldsymbol{q}-\boldsymbol{Q}_{\text{AFM}}} \equiv \langle \mathcal{N}_{\boldsymbol{q}-\boldsymbol{Q}_{\text{AFM}}}\rangle + \delta\mathcal{N}_{\boldsymbol{q}-\boldsymbol{Q}_{\text{AFM}}}$ with $\langle \mathcal{N}_{\boldsymbol{q}-\boldsymbol{Q}_{\text{AFM}}}\rangle = N\Delta S\delta(\boldsymbol{q}-\boldsymbol{Q}_{\text{AFM}})$ and define $m_{\boldsymbol{Q}_{\text{AFM}}} \equiv m \equiv S-\Delta S$ as the reduced sublattice magnetization. Here

$$\Delta S = \frac{1}{N}\sum_{\boldsymbol{q}} \frac{1}{2}\left[\frac{1}{\sqrt{1-\gamma_{\boldsymbol{q}}^2}}-1\right]$$

is the reduction in the ordered spin moment due to zero-point quantum fluctuations and $\gamma_{\boldsymbol{q}}=[\cos q_x+\cos q_y]/2$ comes from the Fourier transform of the exchanges in the square lattice.

The one-magnon dispersion relation is given by

$$\hbar\omega_{\boldsymbol{q}} = 2JZ_C\sqrt{1-\gamma_{\boldsymbol{q}}^2}, \quad (18)$$

where J is the superexchange constant and Z_C is a quantum renormalization of the one-magnon energy, near-constant over the Brillouin zone in a first approximation,[12,13] and estimated as 1.18 to order $1/S^2$ in spin-wave theory[12] or by series expansions.[14]

With these definitions, we can write the longitudinal dynamical structure factor as

$$S_{\text{Hei}}^{zz}(\boldsymbol{q},\omega) = g^2\mu_B^2\Big[Nm^2\delta(\boldsymbol{q}-\boldsymbol{Q}_{\text{AFM}})\delta(\hbar\omega) + \sum_{\nu} |\langle 0|\delta\mathcal{N}_{\boldsymbol{q}-\boldsymbol{Q}_{\text{AFM}}}|\nu\rangle|^2 \delta(\hbar\omega - E_\nu + E_0)\Big], \quad (19)$$

where the first term in the brackets is the Bragg elastic contribution of the Néel order and the second term is the inelastic contribution.

The sublattice magnetization is well known to be accurately given by linear SWT,[15] therefore we do not expect significant changes on the elastic intensity if higher-order corrections are included. In contrast, how the inelastic part is distributed at low energies (a few J's) is expected to be sensitive to such corrections.

The inelastic part can be decomposed into a sum over inelastic processes out of which the dominant term corresponds to two-magnon scattering events with intensity given by[16]

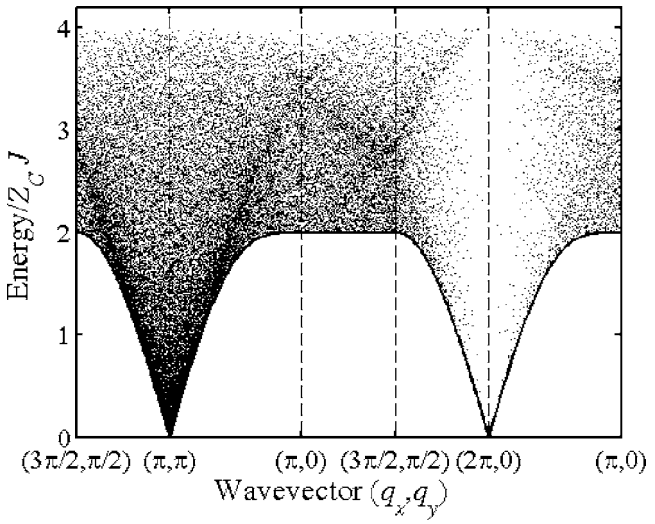

FIG. 1. Two-magnon scattering intensity [Eq. (20)] as a function of energy and wave vector along symmetry directions in the Brillouin zone (solid lines in Fig. 2 inset). Density of scattered points represents intensity. The lower boundary traces the one-magnon dispersion relation $\hbar\omega_{\boldsymbol{q}}$ and corresponds to events where one of the two magnons has zero energy. The upper bound, $4Z_CJ$, is reached when both magnons are on the antiferromagnetic zone boundary contour (dashed square in Fig. 2 inset) where they have maximum energy.

$$S^{zz}_{2M}(\boldsymbol{q},\omega) = Z_{2M}\frac{g^2\mu_B^2}{2N}\sum_{\boldsymbol{q}_1,\boldsymbol{q}_2} f(\boldsymbol{q}_1,\boldsymbol{q}_2)\,\delta(\hbar\omega-\hbar\omega_{\boldsymbol{q}_1}-\hbar\omega_{\boldsymbol{q}_2}) \times \delta(\boldsymbol{q}+\boldsymbol{q}_1-\boldsymbol{q}_2). \quad (20)$$

The two-magnons have opposite spin $S_z=+1$ and -1 such that the total spin S^z_T is unchanged. The scattering cross section $f(\boldsymbol{q}_1,\boldsymbol{q}_2)$ depends on the wave vectors of the two magnons via[16]

$$f(\boldsymbol{q}_1,\boldsymbol{q}_2) = \sinh^2(\theta_{\boldsymbol{q}_1}-\theta_{\boldsymbol{q}_2}), \quad \theta_{\boldsymbol{q}} = \frac{1}{2}\tanh^{-1}\gamma_{\boldsymbol{q}}. \quad (21)$$

We have included an *ad hoc* intensity renormalization factor Z_{2M} to be discussed below. The line shapes in Eq. (20) can be evaluated by direct summation or Monte Carlo methods and the result is illustrated by the dotted areas in Fig. 1.

Two-magnon events contribute a continuum band of scattering at energies above the one-magnon dispersion $\hbar\omega_{\boldsymbol{q}}$. In general, the intensity decreases with increasing energy and it is strongest for wave vectors near the antiferromagnetic zone center (π,π).

Figure 2 shows how the energy-integrated intensity varies in the Brillouin zone, generally following the same trend as the one-magnon intensity. The two-magnon signal cancels at the nuclear zone center $(2\pi,0)$ as expected from first-moment sum rules for an isotropic antiferromagnet, also made apparent from Eq. (21), where the cross section for creating two identical magnons cancels, i.e., for $\boldsymbol{q}_1=\boldsymbol{q}_2$ such that $\boldsymbol{q}=0$, $f(\boldsymbol{q}_1,\boldsymbol{q}_1)=0$.

Figure 3 shows the wave-vector-integrated intensity: it increases with increasing energy, linearly at low energies, then reaches a maximum at the one-magnon zone boundary and then decreases to zero at energies above twice the maximum magnon energy. In fact, most of the two-magnon scattering weight is at energies above the one-magnon cutoff $2Z_CJ$.

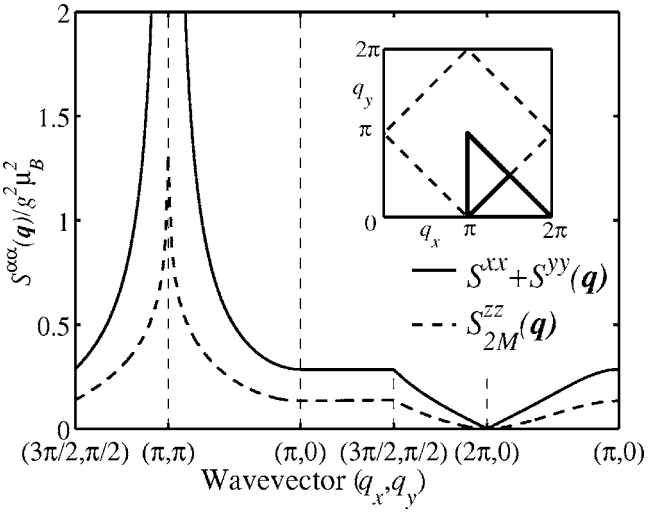

FIG. 2. Energy integrated spectral weight in the two-magnon continuum (dashed line), $S^{zz}_{2M}(\boldsymbol{q})=\int d(\hbar\omega)S^{zz}_{2M}(\boldsymbol{q},\omega)$, compared with the weight in the one-magnon peak (solid line), from Eq. (22). We have used $Z_d=0.57$ and $Z_{2M}=0.67$.

Due to the broadness of the distribution, the two-magnon spectral weight will be quite hard to detect in unpolarized neutron experiments, although we note that recent neutron experiments[17] have observed such a high-energy continuum of excitations in the square-lattice spin-$\frac{5}{2}$ Heisenberg antiferromagnet Rb_2MnF_4 and the observed intensities were in agreement with neutron scattering by pairs of magnons as described by spin-wave theory. In cuprates, in addition, a large fraction of the spectral weight is at energies that are too high for neutron scattering.

Integrating Eq. (20) over energy and wave vector in a Brillouin zone gives $Z_{2M}\Delta S(1+\Delta S)g^2\mu_B^2$, whereas the Bragg elastic scattering is $(S-\Delta S)^2g^2\mu_B^2$. The magnetization reduc-

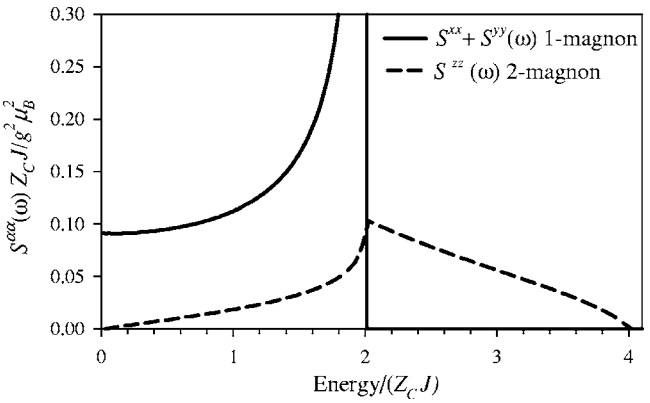

FIG. 3. Momentum integrated spectral function of one- [Eq. (22)] and two-magnon excitations [Eq. (20)]. We have used $Z_d=0.57$ and $Z_{2M}=0.67$. Integrated areas are $(1+2\Delta S)Z_dS$ and $Z_{2M}\Delta S(1+\Delta S)$, respectively.

TABLE I. Sublattice magnetization $m_{\mathbf{Q}_{\mathrm{AFM}}}$ and dynamical structure factor spectral weights in units of μ_B^2. We show exact values for the Ising AFM and SWT values for the Heisenberg AFM in the longitudinal channel (z) and in one transverse channel (x). SWT are the values neglecting all renormalization factors ($Z=1$). We also include the SWT intensity renormalized by the indicated Z values. The transverse contribution is split in the contribution from the magnetic zone and the nuclear zone as $M^x_{\mathrm{MBZ}}+M^x_{\mathrm{NBZ}}$. Since we are considering the Heisenberg model ($D=0$), a "1" in the last column implies that the sum rule is exactly satisfied within the model.

	α	$m_{\mathbf{Q}_{\mathrm{AFM}}}$	Elastic	Inelastic	M_0^α
Ising	z	0.5	1	0	1
	x		0	0.5+0.5	1
SWT	z	0.3034	0.368	0.941[a]	1.309
	x		0	1.068+0.325[b]	1.393[b]
$Z_{2M}=0.67$	z	0.3034	0.368	0.632[a]	1
$Z_d=0.57$[c]	x		0	0.609+0.185[b]	0.794[b]

[a]Two-magnon contribution.
[b]One-magnon contribution.
[c]After Refs. 12 and 18.

tion can be evaluated numerically as $\Delta S=0.197$. The corresponding value of M_0^z is shown in Table I. Comparing with the Ising AFM, also shown in Table I, one sees that the effect of the transverse fluctuations is to reduce the sublattice magnetization with a concomitant transfer of spectral weight from the Bragg peak to the two-magnon continuum. Most of the longitudinal scattering is in this spread-out two-magnon continuum. The spin-only sum rule $M_0^z=1\mu_B^2$ is strongly violated if intensity renormalization is neglected ($Z_{2M}=1$). Notice that if transverse fluctuations are neglected (Ising limit), the sum rule is exactly satisfied. We can anticipate a similar result in the Hubbard model.

Including higher-order terms in spin-wave theory is expected to produce (i) intensity-lowering of the two-magnon response[18] and (ii) spread out at higher energies due to the contribution of higher multimagnon process.[19] For simplicity, we assume the intensity renormalization of the two-magnon response to be momentum-independent and quantify it with the constant Z_{2M}.

Since the Bragg intensity is given accurately by SWT, one can get an upper bound for Z_{2M} by neglecting effect (ii) and requiring that the sum rule Eq. (7) is fulfilled by Bragg and two-magnon processes: $Z_{2M}\sim 0.67$. Perturbative computations[18] suggest a value not far from that, suggesting that the weight in four-magnon and higher multimagnon processes is not high, in agreement with numerical data.[19] In the following, to improve the values of the two-magnon intensity, we tentatively adopt $Z_{2M}=0.67$ given the lack of better estimates (Table I).

It is interesting to remark that the small weight at four-magnon and higher multimagnon processes is in striking contrast to the response relevant for infrared experiments, which show large weights instead.[20–25] From a theoretical point of view, whereas magnon-magnon interactions have dramatic consequences in the shape of the spectrum of two-magnon excitation relevant for Raman and IR data,[21,22] the effect on the two-magnon line shape relevant for magnetic neutron scattering appears much modest.[18] This different role of interactions can be traced back to the fact that optical data probe two magnons in different sublattices whereas magnetic neutron scattering probes two magnons on the same sublattice[22] and the interaction is dominant in the first case. The corresponding Green functions at the RPA level for both cases are reported in Ref. 22. In optical data, magnon-magnon interactions are responsible for a shift of the main feature from $\sim 4J$ to $\sim 3J$.[21,22,26] This effect was obtained in Ref. 22 using a high-energy approximation. One can easily see from the RPA equations for the equal-sublattice Green function[22] that at the same level of approximation the same effect does not show up in the two-magnon neutron-scattering line shape. We conclude that interaction effects should be important for the intensity renormalization but they play a very different role here than the one played in optical data.

2. Transverse part

The transverse dynamical structure factor is dominated by one-magnon scattering events with intensity given by[15]

$$S^{xx}_{\mathrm{Hei}}(\mathbf{q},\omega)=g^2\mu_B^2 Z_d\frac{S}{2}\frac{1-\gamma_{\mathbf{q}}}{\sqrt{1-\gamma_{\mathbf{q}}^2}}\delta(\hbar\omega-\hbar\omega_{\mathbf{q}}), \qquad (22)$$

Z_d is an intensity-lowering renormalization factor of the one-magnon cross section due to zero-point fluctuations and magnon-magnon interactions, both neglected at first order in spin-wave theory [$Z_d=Z_\chi Z_C$, where Z_χ is the renormalization of the transverse magnetic susceptibility, $\chi_\perp=Z_\chi(g\mu_B)^2/8J$].

The wave-vector dependence of the one-magnon intensity is shown in Fig. 2. Although wave vectors $(2\pi,0)\equiv(0,0)$ and (π,π) are related by symmetry, the spectral weight goes to zero at wave vector $(2\pi,0)$ and diverges at (π,π). This difference in intensity is reflected also in doped phases.

Integrating Eq. (22) over energy and wave vector in a Brillouin zone gives the one-magnon intensity for one transverse direction as $(1+2\Delta S)Z_d S g^2\mu_B^2/2$. Experimental works often restrict to the magnetic Brillouin zone around (π,π) (dashed line in the inset of Fig. 2), hereafter "the magnetic Brillouin zone,"(MBZ) and neglect the small weight on the magnetic Brillouin zone around (0,0), hereafter "the nuclear Brillouin zone"(NBZ). For comparison, we split the one-magnon spectral weight in the two zones $M_0^x=M^x_{\mathrm{MBZ}}+M^x_{\mathrm{NBZ}}$. One finds the values reported in Table I.

In this case, as in the longitudinal channel, the sum rule is overestimated if one neglects the intensity renormalization. Estimates of the renormalization from higher-order spin-wave theory give[12,18] $Z_d=0.57$ at order $1/S^2$, or 0.61(4) by series expansions.[14] Now the sum rule is underestimated. The lacking weight is expected to lie in three-magnon and higher multimagnon processes.

An alternative way to estimate Z_d is to enforce Eq. (3) at large S and extrapolate to $S=\frac{1}{2}$. With the choice $Z_d=1-\Delta S/S=0.606$, the total sum rule $S(S+1)$ [cf. Eq. (3)] is exhausted by elastic $(S-\Delta S)^2$, one-magnon $(1+2\Delta S)(S-\Delta S)$, and two-magnon scattering $\Delta S(1+\Delta S)$ (without renor-

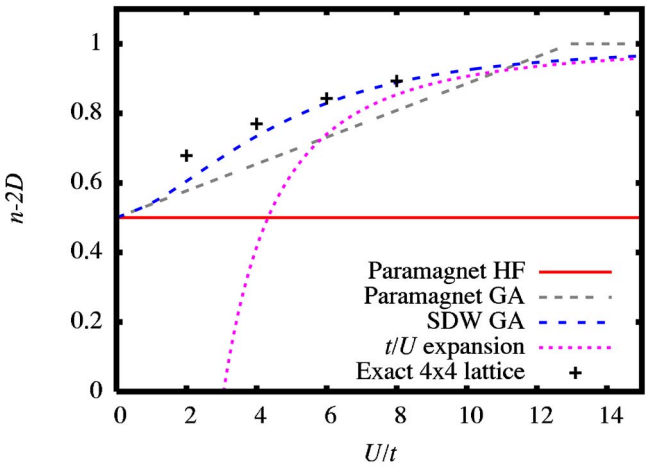

FIG. 4. (Color online) Single occupation probability (shielding factor) for a half-filled Hubbard model in different approximations. The exact results in a 4×4 site cluster are computed with the double occupancies given in Ref. 27. The apparent lack of extrapolation of the exact results to the noninteracting limit at $U=0$ is due to a finite-size effect.

malization), in units of $g^2\mu_B^2$. Such a renormalization of the one-magnon intensity is very close to the results quoted above. Strictly speaking, this argument applies only for $S>\frac{1}{2}$ since the sum rule for each channel Eq. (8), which is exclusive of spin-$\frac{1}{2}$ systems, is still strongly violated. On the other hand, the rapid convergence of the $1/S$ expansions often produces accurate results for $S=\frac{1}{2}$ systems, as seems to be the case for Z_d.

B. Shielding factor in the Hubbard model

We now turn to the more realistic Hubbard model. In this section, we estimate the shielding factor for $n=1$, within the 2D single-band Hubbard model Eq. (4), to gain some insight into its impact on the sum rule Eq. (9). Here we take for simplicity $t'=0$ and consider the effect of varying U/t. Parameters more specific for the cuprates will be considered in Sec. IV.

The shielding factor is given by the single occupancy probability $n-2D$. For a noninteracting system, i.e., $U=0$, the double occupancy is just $(n/2)^2$ so one gets $n-2D=\frac{1}{2}$. Indeed, half of the time an atom is singly occupied (up or down) and half of the time it is either empty or doubly occupied and hence does not produce scattering.

For a paramagnetic state in the Hartree-Fock approximation (HF), one gets the same result independently of U/t (Fig. 4) since correlations are neglected. Correlations can be introduced by treating the paramagnet in the Gutzwiller approximation (GA),[28] which leads to a reduction in double occupancy as

$$D=\frac{1}{4}\left(1-\frac{U}{U_c}\right)$$

becoming zero at the Brinkman-Rice transition point $U_c/t=128/\pi^2\simeq12.97$.[28,29] The corresponding value of $n-2D$ is also plotted in Fig. 4. The Brinkman-Rice point, however, is never reached since for infinitesimal U the paramagnetic state is unstable towards a spin-density wave (SDW), which can also be treated in the GA and gives the value of $n-2D$ shown in Fig. 4.

Finally, for large U/t one can use a canonical transformation to map the Hubbard model to a Heisenberg model.[15,29] It is important to realize that the energies of the low-energy excitations of both models, the "physical" Hubbard model and the low-energy "effective" model, coincide to leading order but the correlation functions in general do not coincide. In order to get "physical" correlation functions, one needs to use the inverse canonical transformation to transform back the "effective" ground-state wave function to a physical wave function. Indeed, within the Heisenberg model the double occupancy is zero, but this does not mean that the double occupancy is zero in the "physical" model. This is obviously very important in evaluating the right-hand side of Eq. (8). Of course if we are interested in evaluating the sum rule *within* the Heisenberg model, it is legitimate to take $D=0$, as done above, but if we want to compare with experiments (or with the "physical" model) one needs to compute the "physical" double occupancy. Fortunately this is very easy in the present case because we can use a trick to avoid the back transformation. We use the Hellman-Feynman theorem to write the double occupancy in the Hubbard model as

$$D=\frac{1}{N}\frac{\partial E}{\partial U}$$

with E the ground-state energy. For the latter we use the fact that for large U/t it coincides with the energy of the Heisenberg model where very accurate numerical estimates exist,

$$\frac{E}{N}=-\left(\alpha+\frac{1}{2}\right)\frac{4t^2}{U},$$

Here we have substituted the superexchange constant by its definition $J\equiv4t^2/U$. The $1/2$ factor is a constant contribution from the canonical transformation and the best estimate for α is $\alpha=0.6696$.[15] Since the Heisenberg model has only one parameter, it is clear that α does not depend on J and we can perform the derivative to obtain

$$D=\left(\alpha+\frac{1}{2}\right)\frac{4t^2}{U^2}.$$

The corresponding value of the single occupancy probability $n-2D$ is plotted in Fig. 4 and referred to as the "t/U expansion." This value is asymptotically exact (within numerical accuracy[15]) in the large U/t limit and therefore takes into account all fluctuation effects. Clearly the SDW treated within the GAs gives a fairly good approximation for $n-2D$ at large U and interpolates smoothly to the exact result at $U=0$ so we expect it to be quite accurate in all the range of U/t, as can be seen also by comparing with the exact results in a 4×4 cluster (after Ref. 27).

We see that the sum rule for one diagonal component of the dynamical structure factor Eq. (8) changes smoothly from $\mu_B^2/2$ in the noninteracting case to μ_B^2 in the limit of

TABLE II. Spectral weights in units of μ_B^2. We show exact values for the Hubbard in the longitudinal channel (z) and in one transverse channel (x). The inelastic weight is separated in the low-energy part (Low) at energy $\sim J$ and the high-energy part $M_{0,U}$ around energy $\sim U$. We also show the sublattice magnetization $m_{\mathbf{Q}_{\mathrm{AFM}}}$ and the shielding factor $n-2D$, both computed in the GA (without RPA correction).

				Inelastic			
U	α	$m_{\mathbf{Q}_{\mathrm{AFM}}}$	Elastic	Low	$M^{\alpha}_{0,U}$	M^{α}_{0}	$n-2D$
8	z	0.43	0.74	0	0.15	0.898	0.889
	x		0	1.1	0.01	1.11	
10	z	0.456	0.83	0	0.096	0.930	0.923
	x		0	1.196	0.009	1.205	
15	z	0.481	0.927	0	0.0397	0.966	0.965
	x		0	1.278	0.002	1.28	

$U=\infty$. It is reduced by $\sim 11\%$ (Table II) with respect to the full moment value for $U/t\sim 8$, as relevant for cuprates.[30,31]

C. Distribution of spectral weight in the Hubbard model

In the previous section we evaluated the shielding factors that appear due to the finiteness of U and reduce the total spectral weight compared to spin-only models. Another effect, which we study here, is that the total weight is split into a low-energy part at energies of order J and a high-energy part at energies of order U. Present neutron-scattering facilities can measure the spectra up to energies of the order of a few tenths of an eV and therefore only the first part is detected. In addition, we discuss how the dynamical structure factor is modified for finite U with respect to the SWT result.

To estimate the dynamical structure factor, we use the time-dependent Gutzwiller approximation of Refs. 7–9 [also called GA plus random-phase-approximation (GA+RPA)] applied to a SDW state. We start in the next section by showing how measurements of the dispersion relation in the insulator can be used to estimate U and t.

1. Transverse part

In the transverse channel, MNS experiments reveal the spin-wave excitations of the AFM.[30] Interestingly, whereas spin-wave theory in the Heisenberg model Eq. (18) predicts a flat dispersion between $(\pi,0)$ and $(\pi/2,\pi/2)$, a substantial dispersion has been measured (cf. Fig. 5). It has been argued that in cuprates, corrections to the Heisenberg model arising as higher orders in a t/U expansion are relevant.[25,30,32–34] The most important of such corrections is a term that cyclically exchanges four spins on a plaquette. A sizable value for this term has been revealed by analyzing phonon-assisted multimagnon infrared absorption[25] and the dispersion relation[30] shown in Fig. 5. In particular, the dispersion between $(\pi,0)$ and $(\pi/2,\pi/2)$ is mainly due to this term. Since the dispersion has its origin in the finiteness of t/U, it should show up in the transverse excitations of the Hubbard model. The computation done in GA+RPA is also shown in Fig. 5. One obtains a very good fit of the dispersion, and this provides an accurate way to estimate the strength of the repulsion. We find $U/t=8$ in good agreement with other estimates,[30] whereas $U/t=10$ gives a too flat dispersion between $(\pi,0)$ and $(\pi/2,\pi/2)$ (inset). An equally good fit as the one shown in the main panel can be achieved with $U/t=8$, $t'/t=-0.2$, and $t=353.7$ meV. The value of t'/t plays an important role in the doped phase[31,35] and is close to a first-principle estimate.[36]

In Fig. 6, we show the momentum integrated spectral function. We see that for large U/t it approaches the SWT form (Fig. 3). For smaller U/t the maximum is not at the upper edge due to the modified dispersion relation. A small portion of the spectral weight is at high energy due to spin-flip transitions from the lower to the upper Hubbard band as shown in the inset. We will show that this effect is much larger in the longitudinal channel.

Integrating the spectral intensity, one gets the values of M_0^x shown in Table II. GA+RPA interpolates between the extreme limits $U/t=0$ (where the sum rule is exactly obeyed) and $U\to\infty$ where one recovers the results of linear spin-wave theory. As a consequence, the sum rule in the transverse channel is increasingly violated as U/t increases with

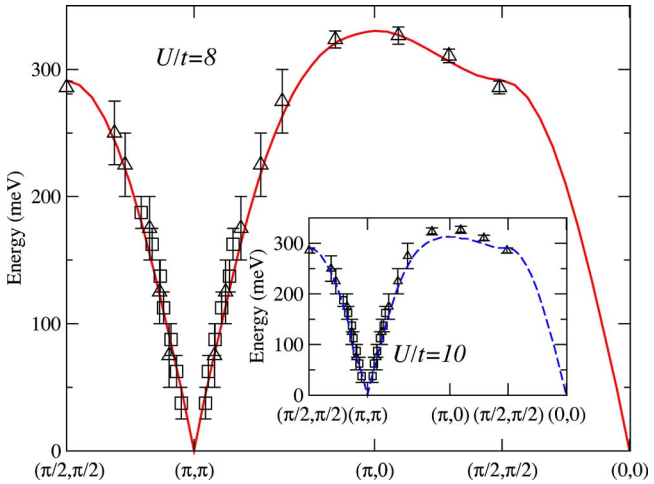

FIG. 5. (Color online) Dispersion relation of the low-energy transverse excitations. We show the experimental result for La_2CuO_4 after Ref. 30 and the GA+RPA result for $U/t=8$ and $t=335$ meV. The inset shows that for $U/t=10$ the fit is noticeably worse.

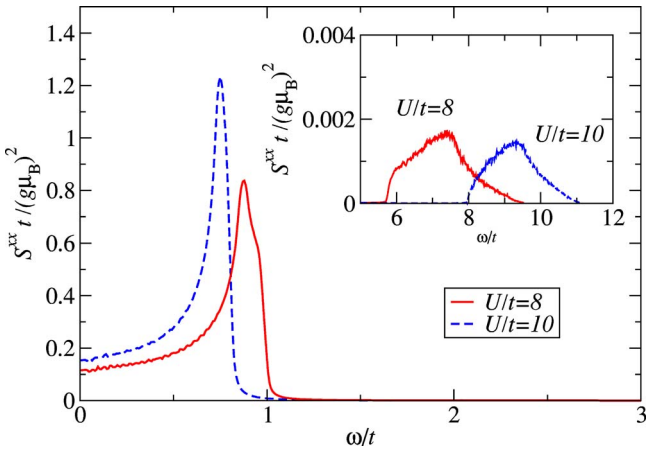

FIG. 6. (Color online) $S^{xx}(\omega)$ evaluated for the Hubbard model within GA+RPA for $U/t=8$ (solid line) and $U/t=10$ (dashed line) with $Z_d^U=1$ for an (80×80)-site system. The inset shows the high-energy contribution of $S^{xx}(\omega)$ at energies $\omega\sim U$.

M_0^x reaching values similar to the unrenormalized SWT results (Table I) for large U.

In Fig. 7, we show the experimental intensities as a function of wave vector together with the GA+RPA result. In order to fit the experimental results, we introduced an intensity renormalization $Z_d^{U=8t}$ analogous to the SWT intensity renormalization factor. With $Z_d^{U=8t}=0.65$, the GA+RPA intensities are essentially equivalent to the intensities reported in Fig. 3(b) of Ref. 30, which have been renormalized by $Z_d^{\mathrm{exp}}=0.51$ *with respect to LSWT*.

This increase in the value of Z_d^U reflects the fact that cuprates are not in the strict Heisenberg limit $U\to\infty$. In that limit, the Z_d for the RPA should coincide with the value of LSWT given the equivalence of the two approximations. In the extreme case of a noninteracting system, the RPA gives exact intensities and therefore $Z_d^{U=0}=1$. As U is decreased

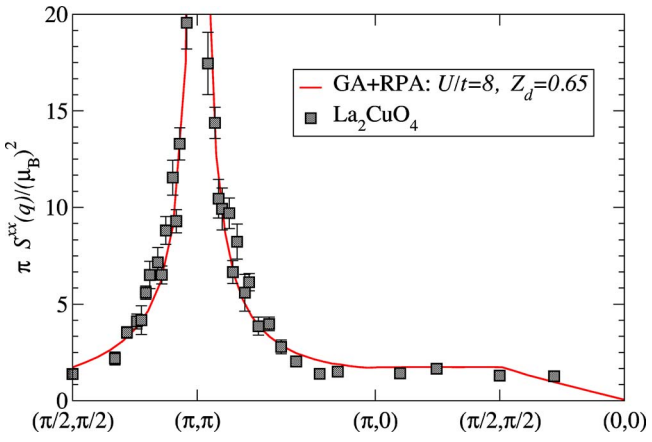

FIG. 7. (Color online) Intensity in the spin-wave excitations as a function of momentum for one transverse spin channel. We show the experimental result for La_2CuO_4 after Ref. 30 and the GA+RPA result for $U/t=8$ and $t=335$ meV. The GA+RPA intensity has been renormalized by a factor $Z_d^{U=8t}=0.65$ and coincides with the spin-wave result [shown in Fig. 3(b) of Ref. 30] renormalized by $Z_d^{\mathrm{exp}}=0.51$ in Eq. (22).

from infinity, the RPA becomes gradually more accurate and therefore Z_d^U should increase with respect to the LSWT value, as we indeed find.

We caution that the fact that a system is not in the strict Heisenberg limit does not mean by itself that it cannot be described by the Heisenberg model. Corrections to the intensity can be introduced as explained in Sec. III D. We estimate this approach is accurate up to $U\sim15t$ where the dispersion is still Heisenberg-like. For smaller U, corrections in the dispersion relation due to four spin exchange and other non-Heisenberg processes become obvious (cf. Fig. 5).

2. Longitudinal part

The longitudinal structure factor has a Bragg part and an inelastic part [cf. Eq. (12)]. For the SDW, only one magnetic reciprocal-lattice vector contributes to the sum in Eq. (12), namely $\boldsymbol{Q}_{\mathrm{AFM}}\equiv(\pi,\pi)$ (we take the lattice constant $a=1$). The Bragg weight is determined by the sublattice magnetization $m_{\boldsymbol{Q}_{\mathrm{AFM}}}$.

At lowest order the RPA introduces longitudinal fluctuations in S^{zz} but does not correct one-body expectation values like the sublattice magnetization. (On the contrary, it introduces a correction in two-body expectation values[7] like D.) Therefore, in the following we consider the sublattice magnetization at the GA level together with the effect of the longitudinal fluctuations at high energies in S^{zz}. The sublattice magnetization can in principle be corrected by including transverse fluctuations. We will discuss this below.

At the GA we obtain the values of the sublattice magnetization shown in Table II. These values lack the transverse fluctuation corrections and hence converge to the classical value, 0.5 in the large-U limit.

To help our intuition, it is useful to distinguish between the permanent moment $m=|\langle n_{i\uparrow}-n_{i\downarrow}\rangle|/2$, which determines the Bragg weight, and an "intrinsic" moment which determines the shielding factor and which we define as $m^*=\sqrt{\langle(n_{i\uparrow}-n_{i\downarrow})^2\rangle}/2=\sqrt{(n-2D)}/2$. (Notice that with this definition a free fermion system has an intrinsic moment which we denote as "trivial.") The paramagnet with small D mentioned in Sec. III B can be considered as a system with well formed (nontrivial) intrinsic moments that are purely dynamical. Indeed the shielding factor is close to 1 but there are no Bragg peaks. In this regard, the GA is more flexible than HF, which is not able to produce nontrivial intrinsic moments that are not permanent.

Permanent moments are due to the breaking of spin-rotational symmetry. The GA for the SDW smoothly interpolates between the itinerant limit at small U and the localized limit at large U with a permanent moment that increases and reaches $\frac{1}{2}$ for $U\to\infty$. Contrary to the paramagnetic case, quoted above, the difference between the permanent and the intrinsic moment in the GA tends to be very small at large U. Thus despite the ability of the GA to distinguish the two kinds of moments, this ability is not effective at large U. In this case, the permanent moment in the GA (cf. Table II) is reduced with respect to the fully polarized value mainly due to covalency effects. On top of this, the moment will be reduced due to transverse fluctuations, as discussed below.

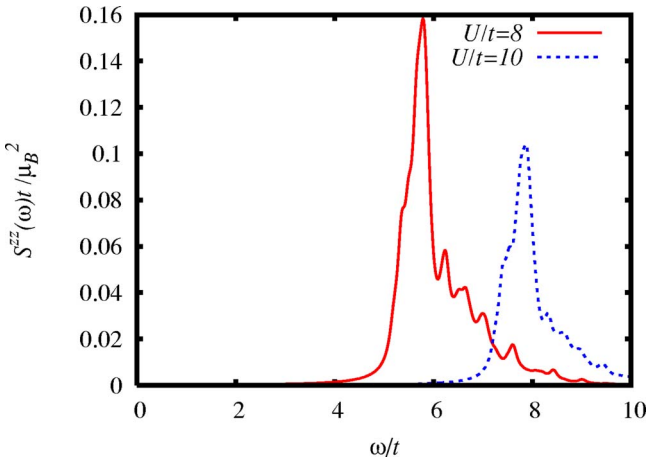

FIG. 8. (Color online) Inelastic part of $S^{zz}(\omega)$ in the GA+RPA for different values of U/t in an (8×8)-site system.

The covalency reduced Bragg peak does not exhaust the sum rule, as can be seen by comparing the "Elastic" column with the last column in Table II. Longitudinal fluctuations, captured by the GA+RPA approach, produce weight at energies of order U, as shown in Fig. 8. This is not related to two-magnon processes (as in Sec. III A 1) but to fluctuations in the length of the intrinsic moment. The weight in the high-energy part $M_{0,U}$ is also reported in Table II. Adding the Bragg and the $M^z_{0,U}$ contribution, one obtains the values of M^z_0 reported in Table II. Comparing with the last column, we see that at this level of approximation the sum rule is exhausted (actually slightly overshot) by the Bragg contribution without transverse fluctuation reductions plus the contribution at energy of order U.

The small overshot in the sum rule is due to the fact that the last column is computed at the GA level without RPA corrections, whereas M^z_0 has RPA corrections to D. (An analogous method was used in Ref. 7 to compute fluctuation corrections to D.) The M^z_0 column can be considered as an improved computation of the shielding factor. We see that the difference is very small and for practical purposes we can use the GA result.

From the above results, it is clear that in neglecting transverse fluctuations the sum rule is well satisfied. This is analogous to the behavior found for the spin-only model in the Ising limit (Table I).

At this point, we have weight at the Bragg peak and weight at energy of order U. How do these weights get affected by transverse fluctuations? On top of the covalency reduction, transverse fluctuations reduce the permanent moment (keeping the intrinsic moment constant). We have seen above (Sec. III A 1) that the reduction of the moment due to transverse fluctuations produces a concomitant large reduction of elastic spectral weight which is transferred to multimagnon processes in the longitudinal channel at energy $\sim J$. A direct computation in the Hubbard model is difficult. In the next section, we show how to estimate this effect in the Hubbard model using the SWT results.

We expect that this low-energy rearrangement of spectral weights will affect neither $M^z_{0,U}$ nor the shielding factor computed above, which, as is clear from Fig. 4, is quite accurate at the present level of approximation. Therefore, we expect the present values of $(n-2D)\mu_B^2 - M^z_{0,U}$ and $M^z_{0,U}$ (without transverse fluctuations) to be accurate estimates of the total spectral weight at low (order J) and high (order U) energies.

D. Effective shielding factor

In this section, we would like to show how to use the spin-wave theory results together with the results of the previous section to obtain a better distribution of the spectral weight.

According to the discussion of Sec III B, to obtain the "physical" dynamical structure at low energies from the Heisenberg model response, one should apply the canonical transformation back from the effective model to the Hubbard model. Since the processes involved in a t/U expansion have a short spatial range and involve intermediate states at high energies, we do not expect this procedure to lead to a momentum or low-energy-dependent correction. Thus the "physical" dynamical correlation functions at low energy can be obtained from the requirement that the sum rule is satisfied as

$$S^{\alpha\alpha}(q,\omega) = (n - 2D - M^{\alpha}_{0,U}/\mu_B^2) S^{\alpha\alpha}_{\mathrm{Hei}}(q,\omega), \qquad (23)$$

where $S^{\alpha\alpha}_{\mathrm{Hei}}(q,\omega)$ is the dynamical correlation function of the Heisenberg model and $M^{\alpha}_{0,U}$ is the weight transferred to high energies due to the finiteness of U computed in Sec. III C. Alternatively, a model with higher-order corrections (ring exchange, etc.) can be taken to compute the response on the right-hand side of Eq. (23).

We can consider $(n-2D-M^{\alpha}_{0,U}/\mu_B^2)$ in Eq. (23) as an effective shielding factor for low-energy spectral weight. One can check from the results of Table II that this works for the Bragg intensities neglecting transverse fluctuations. Indeed, we have

$$4m^2_{Q_{\mathrm{AFM}}}\mu_B^2 = (n - 2D)\mu_B^2 - M^z_{0,U}, \qquad (24)$$

where the left-hand side is the Bragg weight in the GA for the Hubbard model without RPA correction and the right-hand side is the effective shielding factor times the Bragg weight in the Ising limit of the spin-only model $(1\mu_B^2)$.

Due to the separation of energy scales, D and $M^z_{0,U}$ will be insensitive to transverse fluctuations. The effect of the latter will be to transfer weight from the Bragg peak to the low-energy continua without affecting the total low-energy spectral weight. Thus Eq. (24) tells us that the total low-energy spectral weight (Bragg plus multimagnon contribution) is accurately given by the mean-field value $4m^2_{Q_{\mathrm{AFM}}}\mu_B^2$.

As a corollary, we see that a good estimate of the longitudinal effective shielding factor is given by the moment in the GA without the need of an RPA computation, i.e., the low-energy part of the longitudinal dynamical structure factor gets rescaled by the mean-field value of $4m^2_{Q_{\mathrm{AFM}}}$. This is consistent with the findings of Hirsch and Tang from numerical data[37] if one takes into account that the HF approximation, used by Hirsch and Tang, gives very similar values of $m_{Q_{\mathrm{AFM}}}$ as the GA in the range of U analyzed.

In Fig. 9, we show the two-magnon contribution computed in the Heisenberg model and translated into a Hubbard

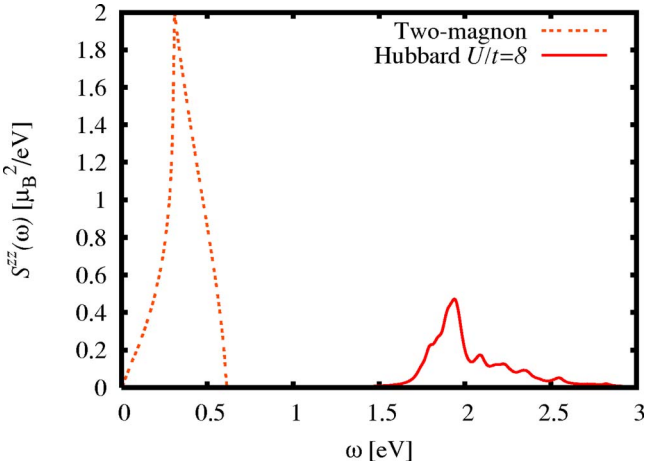

FIG. 9. (Color online) Momentum integrated longitudinal spectral function for the Hubbard model with $U=8t$, $t=335$ meV, and $Z_c J=153$ meV. We show the contribution of two-magnon excitations computed in SWT [Eq. (23)] with an effective shielding factor of 0.74 (Table II) and $Z_{2M}=0.67$. We also show the contribution due to scattering across the Hubbard bands computed in GA+RPA.

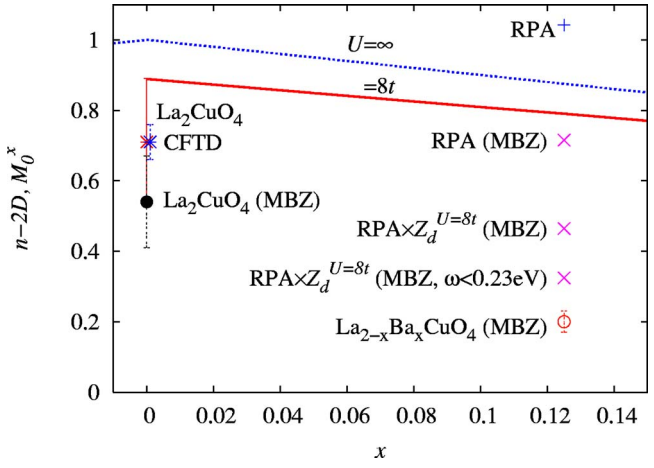

FIG. 10. (Color online) Zeroth moment and shielding factor as a function of doping. We show the shielding factor for $U/t=8$ and $t'/t=-0.2$ for the SDW at $x=0$ and bond-centered metallic stripe solutions as a function of doping (solid line) and for $U/t=\infty$ (dotted line). For the zeroth moment, MBZ means that the integration was restricted to the magnetic Brillouin zone. La_2CuO_4 (Ref. 30) and CFTD (Ref. 40) label the moments estimated in insulators (Sec. III E). Their value coincide so CFTD was slightly shifted in doping for clarity. $La_{2-x}Ba_xCuO_4$ (Ref. 1) labels the experimental value of M_0 in the magnetic Brillouin zone, corrected by the polarization factor. In the last case, the error bars indicate the two extreme possibilities for the polarization factor 2/3 and 1/2 (cf. Sec. II). The relative true error should be larger than at zero doping, where the error bars have the usual sense. Finally, we show the zeroth moment of the GA+RPA transverse spectra at $x=1/8$ in the whole Brillouin zone (+) and in the MBZ ×. The two lower × include a $Z_d^{U=8t}=0.65$ renormalization factor and for the lower one the energy integration was restricted to energies smaller than 0.23 eV.

response according to Eq. (23), together with the longitudinal response at energy $\sim U$ computed directly in the Hubbard model. Additionally, there is a Bragg peak (not shown) with weight $16m_{\mathbf{Q}_{\mathrm{AFM}}}^2\mu_B^2(S-\Delta S)^2$, where $m_{\mathbf{Q}_{\mathrm{AFM}}}$ is computed at the mean-field level and $4(S-\Delta S)^2$ takes into account the effect of transverse fluctuations. This is our best estimate for the distribution of spectral weight in the longitudinal response of the insulator.

Notice that the transition across the Hubbard bands appears at 2 eV. One should remember that on the mapping from the three-band Hubbard model to the one-band Hubbard model,[38] the transition across the Hubbard bands of the latter represents the charge-transfer transitions of the former, which according to optical data should occur close to ~2 eV.[39] Indeed, in the ionic limit the lower Hubbard band of the one-band model corresponds to O p^6 states and the upper Hubbard band to Cu d^{10}.

E. Estimation of the weights in La_2CuO_4 and $Cu(DCOO)_2\cdot 4D_2O$ (CFTD)

In La_2CuO_4, the dynamical structure factor can be fitted[30] in a wide range of momentum and energy by the SWT expressions Eq. (22) with an intensity-lowering renormalization factor $Z_d^{\mathrm{exp}}=0.51\pm0.13$. We can use this result to estimate the different contributions to the moments for the *one-magnon* processes in La_2CuO_4,

$$M^x_{\mathrm{NBZ}}=0.16\pm0.04\mu_B^2,$$

$$M^x_{\mathrm{MBZ}}=0.54\pm0.13\mu_B^2,$$

and

$$M^x_0=0.71\pm0.18\mu_B^2.$$

The last value should be interpreted as the weight for one transverse direction in the spin-wave-like excitations of La_2CuO_4. This is not the total weight since part of the weight will be in higher multimagnon processes.

The experimental determination of the intensity-lowering factor, Z_d^{exp}, neglected shielding factors. Therefore, the experimentally determined quantity can be set as $Z_d^{\mathrm{exp}}=Z_d^{\mathrm{eff}}=(n-2D-M^x_{0,U}/\mu_B)Z_d$. Using an effective shielding factor for $U/t=8$ as appropriate for La_2CuO_4, $(n-2D-M^x_{0,U}/\mu_B)=0.88$ and $Z_d=0.57$ (SWT), one obtains $Z_d^{\mathrm{eff}}=0.50$ in agreement with the experiment (inclusion of $t'/t=-0.2$ does not change this number appreciably).

Subtracting the observed one-magnon weight from the total expected transverse weight of $0.88\mu_B$ would then leave a total of $0.17\pm0.18\mu_B^2$ in three, five, and higher multimagnon processes, which is within the error bars as illustrated in Fig. 10. Notice that the detected one-magnon spectral weight is significantly lower than $1\mu_B$, the value expected from the sum rule neglecting the shielding factors and quantum corrections.

For $Cu(DCOO)_2\cdot 4D_2O$ (CFTD), Rønnow *et al.*[40] also find $Z_d^{\mathrm{exp}}=0.51\pm0.04$ within LSWT. For this compound the ratio of U/t is much larger than in the cuprates and the shielding factor correction should therefore be close to 1. Since the error bars are smaller than in the cuprates, this experiment shows, not surprisingly, that multimagnon processes are needed to satisfy the sum rule (see Fig. 10). The

similarity for Z_d^{exp} found for the two compounds is to some extent unexpected since there should be a difference due to the shielding factors, however the expected difference is within the current experimental errors. Notice also that g may also differ in the two compounds.

IV. AWAY FROM HALF-FILLING

A. Shielding factors

Taking $g=2$ and defining the doping as $x=1-n$, the shielding factor for general doping changes from $(1-x^2)/2$ for $U=0$ to $1-|x|$ for $U=\infty$, the latter form being used often in experimental works. In general, we expect a dependence on U/t qualitatively similar to the one shown at $x=0$ (cf. Fig. 4).

In order to proceed in the doped phase, we need a model for the ground state. In this work, we are interested in overall distributions of weights and we expect this to be to a large extent insensitive to the details of the ground state if correlations are taken reasonably well into account. This can be seen already at $x=0$ (cf. Fig. 4), where we see that the paramagnet and the SDW within the GA give similar shielding factors although the nature of the ground state is completely different. Detailed distributions of spectral weight as measured in Ref. 1 and computed in Ref. 31 will, of course, depend strongly on the ground state and so can be quite helpful to determine it. Since those issues are beyond our present scope, we restrict the description of the mean-field states to a minimum.

For the specific system $La_{2-x}X_xCuO_4$ (X=Sr,Ba), we use a ground state consisting of stripes as suggested by experiment.[1,41] Metallic stripes parallel to the CuO bond can be obtained within the GA for the Hubbard model where a next-nearest-neighbor hopping $t'/t=-0.2$ has to be implemented in order to have one doped hole per every second unit cell along the stripe[35] (so called "half-filled" stripes) in agreement with experiments. Note that a similar value for t'/t is predicted by first-principle computations[36] for $La_{2-x}Sr_xCuO_4$.

It should be mentioned that the results at half-filling reported in the previous sections are rather insensitive to the next-nearest-neighbor hopping. For $U/t=8$ and $t'/t=-0.2$, we obtain an analogous dispersion to that reported in Fig. 5, with the only difference being that the value for the nearest-neighbor hopping has to be scaled to $t=353.7$ meV. This latter parameter set has been used[31] in order to explain a recent MNS experiment on Ba-codoped LSCO.[1] Overall spectral weights with this extended parameter set are practically the same as those reported in Sec. III C 1 with $t'=0$.

In Fig. 10, we show the shielding factor obtained averaging $(n-2D)$ in the mean-field solutions as a function of doping. We see that the shielding factor has a linear behavior similar to the one for the $U/t=\infty$ case. As expected, we find that the shielding factor is similar for other low-energy textures (not shown). For doping $x=1/8$ we obtain $n-2D=0.79$, so there is an extra 10% reduction with respect to the undoped case.

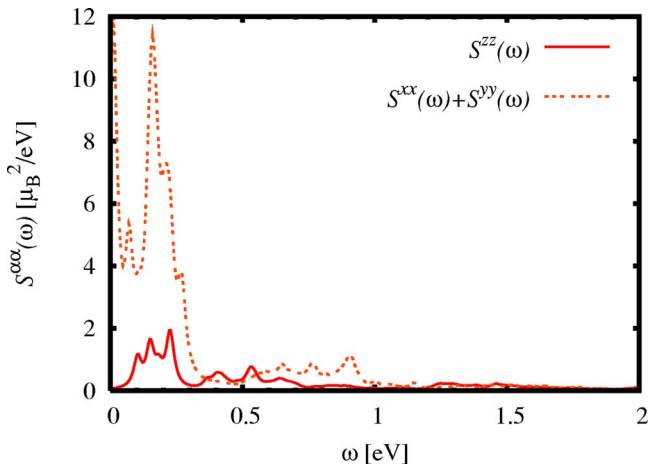

FIG. 11. (Color online) Longitudinal and transverse components of the spin autocorrelation function for $x=1/8$ in a 16×4 site cluster for $U/t=8$ and $t'/t=-0.2$ and $t=353.7$ meV. Only the inelastic part is shown and we neglect the intensity renormalization ($Z=1$). The ground state consists of 4 SC stripe running along the short dimension.

B. Spectral weights

1. Longitudinal part

Because the stripe solutions are magnetic, the longitudinal structure factor has a Bragg part and an inelastic part [cf. Eq. (12)].

Since the stripe solutions are metallic, low-energy particle-hole excitations are allowed. Therefore, contrary to the result in the insulator (Sec. III C 2), already at the RPA level one finds weight at magnetic energies ($\lesssim$0.3 eV) as shown in Fig. 11. This weight, however, is broadly distributed in momentum space and will most likely pass unnoticed in unpolarized MNS as discussed in Sec. II D. Just as shown in Fig. 9, for the insulator a more elaborate computation, taking into account longitudinal fluctuations, will show in addition weight at the two-magnon excitations. Since the inelastic longitudinal component due to multimagnon scattering is already quite featureless in the insulator (Secs. III A 1 and III C 2), it is reasonable to expect that it will be even more featureless in the doped phase. We conclude that within standard protocols (Sec. II D) to a first approximation all the inelastic longitudinal spectral weight will be assigned to the background.

For the specific case of a striped ground state, we can also estimate the elastic spectral weight in the longitudinal channel [Eq. (12)]. For doping $x=1/8$ and an array of $d=4$ SC stripes, we find elastic peaks at $\boldsymbol{Q}_1=(1/2\pm\epsilon,1/2)2\pi$ and $\boldsymbol{Q}_2=(1/2\pm2\epsilon,1/2)2\pi$ with $\epsilon=1/8$ and $m_{Q_1}=0.215$ and very small weight, $m_{\boldsymbol{Q}}^2$, in the higher harmonics $m_{Q_2}=0.018$.

It was shown in the insulator that if one neglects transverse fluctuations, the sum rule in the longitudinal channel is exhausted with a good degree of approximation by the Bragg weight plus the inelastic high-energy weight. Is there an analogous behavior in the doped phase? The elastic weight neglecting transverse fluctuations is $0.37\mu_B^2$ and the inelastic longitudinal spectral weight is $0.59\mu_B^2$. This includes low-

energy particle-hole excitations and weight due to transitions across the Hubbard bands. The total weight in the longitudinal channel is $0.96\mu_B^2$, to be compared with a shielding factor of 0.79. In this case, we find an overstrike of the sum rule which is more severe than in the insulator and which is even larger than the maximum allowed value $1-x=0.875$. This is because the RPA becomes less accurate in the metallic phase due to the presence of small energy denominators. The violation, however, is not as severe as for the transverse channels as reported below.

The elastic weight neglecting transverse fluctuations is roughly half of the one found in the insulator ($0.74\mu_B$). Just as in the insulator, a large fraction of this weight (at least 60%) will be transferred to multimagnon excitations if transverse fluctuations are taken into account. It is conceivable that all the weight in the Bragg peak is transferred, in which case the system becomes quantum critical or quantum disordered.[42]

2. Transverse part

The transverse component of the dynamical structure factor shows sharp features due to the propagating spin-wave-like modes of the stripes. In addition, since the stripes are metallic, a fraction of the spectral weight is in a broad particle hole continuum. The latter features, however, are mainly located in the nuclear Brillouin zone.[31]

In the magnetic Brillouin zone, we find mainly sharp propagating collective modes which are good candidates to be easily detected. These collective modes are analogous to the spin-wave modes of the insulator and therefore we expect that their spectral weight will be overestimated in the RPA and should be corrected by a quantum renormalization Z_d^U as in the insulator. Z_d^U may be smaller than in the insulator due to stronger quantum fluctuations. On the other hand, for a heavily doped system one should recover the noninteracting value $Z_d=1$. Since doping is small, we tentatively take the same value as in the insulator $Z_d^{U=8}=0.65$.

The momentum distribution of the transverse spectral weight has been shown in Ref. 31. In Fig. 10, we show the transverse integrated spectral weight compared with the experimental results. At zero doping, the spectral weight coincides with the theoretical value (not shown for clarity) as discussed in Sec. III. At finite doping, the weight in the MBZ decreases roughly as the shielding factor, as can be seen by comparing the points labeled La_2CuO_4(MBZ) and RPA$\times Z_d^{U=8t}$(MBZ). Comparing Fig. 6 and Fig. 11, we see that whereas in the insulator almost all of the spectral weight is at magnetic energies, in the doped phase a large fraction of the spectral weight is at intermediate energies not accessible to MNS. In other words, doping induces a transfer of spectral weight from low energies to intermediate energies in this channel. Interestingly, optical spectra show that doping also generates structure at the same energies in the charge channel.[39,43,44]

The lower "×" at $x=1/8$ in Fig. 10 is the RPA moment in the MBZ renormalized by $Z_d^{U=8t}$ and restricting the integral only up to the highest energy measured in Ref. 1, $\omega<0.23$ eV. We see that the obtained value is roughly 50% higher than the experimental weight.

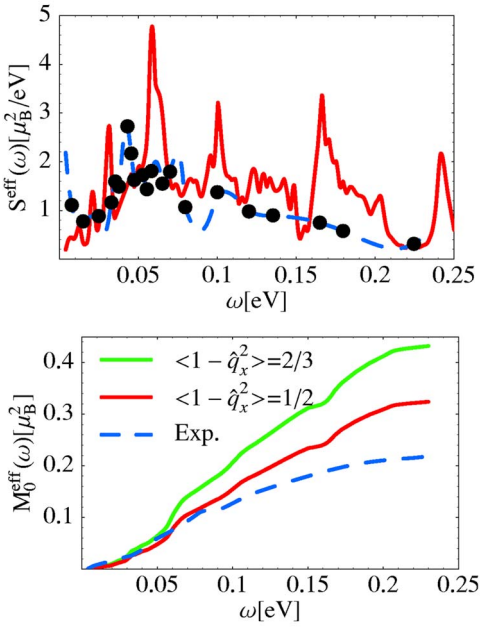

FIG. 12. (Color online) The upper panel shows the theoretical and the experimental result for $S^{\rm eff}(\omega)$ using $U/t=8$, $t'/t=-0.2$, $t=353.7$ eV, and $(1-\hat{q}_x^2)\rangle_{\rm dom}=(1-\hat{q}_y^2)\rangle_{\rm dom}=1/2$, in a (96×96)-site lattice, together with the experimental data for $La_{2-x}Ba_xCuO_4$ $x=0.125$ (Ref. 1). The lower panel shows the partial sum rule weight. $M_0^{\rm eff}(\omega)\equiv(1/N)\Sigma_{\boldsymbol{q}}\int_{-0}^{\omega}d(\hbar\omega')S^{\rm eff}(\boldsymbol{q},\omega')$.

In order to see at what energy the disagreement arises, we show in Fig. 12 the experimental $S^{\rm eff}$ compared with the theoretical one using $\frac{1}{2}$ as polarization factors [Eq. (16)] and neglecting the longitudinal weight. The lower panel shows a comparison of the partial sum rule weight with the two limiting values of the polarization factor. The theoretical computation shows a strong resonance at $\omega=58$ meV which in the experiment appears with a reduced spectral weight and is distributed in part on a broader energy range. (The resonance appears at higher energy if one looks only at the $Q_{\rm AFM}$ response.[31]) The overall weight integrated up to energies immediately above the resonance is in agreement with the experimental one. As the energy increases, there are strong deviations between theory and experiment.

The simplest explanation for the smaller weight in the experiment is that some of the structures that contribute at high energy may be broad and assigned to the background (see Ref. 31). We should say that because we neglect lifetime effects even the sharp structures of our computation will be much broader in reality and this will be more important as the energy increases since, quite generally, the phase space for decay processes increases. Also high-energy excitations will be much more sensitive to disorder since they involve short wavelengths, and this will also tend to make them broader. The broad structures will be assigned to the background explaining the difference between theory and experiment. We should also take into account that Z_d can be more depressed due to the larger impact of quantum fluctuations in the metallic phase.

In order to have a broader view of the trends in the evolution of the spectral weight, we show in Fig. 13 a compila-

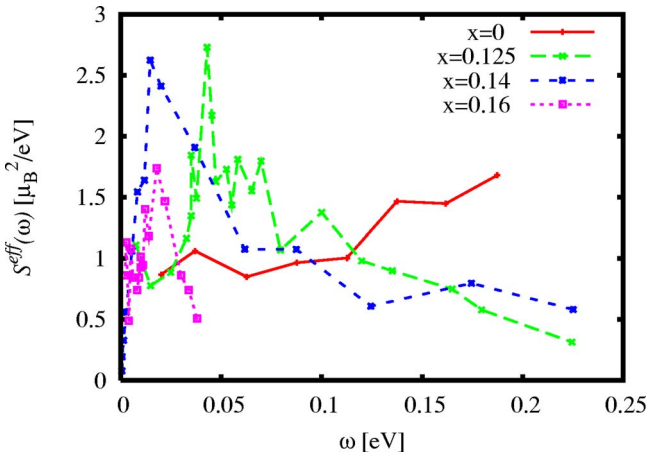

FIG. 13. (Color online) Experimental results for $S^{\mathrm{eff}}(\omega)$ for $x=0$ (Ref. 45), $La_{2-x}Ba_xCuO_4$ $x=0.125$ (Ref. 1), and $La_{2-x}Sr_xCuO_4$ with $x=0.14$ (Ref. 45) and $x=0.16$ (Ref. 46). We used the following conversions from the quantity reported in the quoted reference: $S^{\mathrm{eff}}=S$ (Ref. 1) $=(2/\pi)\chi$ (Ref. 45) $=(2/\pi)\chi$ (Ref. 46).

tion of measurements of S^{eff} from different groups and at different dopings. For $x=0$, 0.125, and 0.14, the overall weight seems to be roughly conserved, whereas for $x=0.16$ the detected weight seems to be significantly smaller. It will be interesting to see whether this is due to a transfer to high energies where absolute measurements are not available. After this work was completed we became aware of Ref. 47 where a systematic decrease of the low energy spectral weight as a function of doping is reported.

V. CONCLUSIONS

In this work, we have analyzed the distribution of spectral weight in neutron-scattering experiments in cuprates.

In the insulator, the spectral weight has been estimated in detail in the Heisenberg model and then translated into a Hubbard response with the use of an effective shielding factor. We find an effective shielding factor which essentially coincides with a proposal of Hirsch and Tang obtained by analyzing numerical data.[37] In addition we have estimated, with the aid of the TDGA, the weight at the energy of the charge-transfer transitions.

The inelastic longitudinal spectral weight at low energies is in broad features and thus hard to detect, although progress has recently been made.[17] The transverse part has the well known quantum renormalized propagating spin wave modes which will be the features more accessible to experiment. Theory and experiment agree well in the insulator.

For the doped phase, we computed the dynamical response within the TDGA. We considered metallic stripes but we expect our results for overall weights to be largely insensitive to the specific texture. One finds extra broad features due to the particle-hole continua plus propagating collective modes. In analogy with the insulator, we expect the latter to be reduced in intensity due to quantum fluctuation and to dominate the spectral weight reported in experiments.

Our motivation was to understand why such a small fraction of the naively expected spectral weight is actually detected. We see that after taking into account all the reduction factors, we passed from a weight that was an order of magnitude smaller than expected to a weight that is $\sim\frac{2}{3}$ of that expected. Given the uncertainties involved, we think this value is reasonable.

By far the most important factor in reducing the detectable weight turns out to be the fact that a large fraction of the spectral weight is in broad features or at too high energies and this makes the detection of the total spectral weight experimentally very challenging. In the doped phase, a consistent fraction of the transverse spectral weight is predicted to lie at intermediate energies, which may become accessible to experiment in the near future.

We see no reason why the broad/high-energy modes cannot have a strong impact on the effective attraction between holes relevant for superconductivity, and therefore their experimental characterization remains an important open problem.

ACKNOWLEDGMENTS

We acknowledge support from the UK EPSRC under Grant No. GR/R76714/01 (R.C.). J.L. thanks the University of Oxford, ISIS, and the CCLRC's Rutherford Appleton Laboratory for financial support and hospitality during part of this work, and A. T. Boothroyd, S. M. Hayden, D. F. McMorrow, T. G. Perring, and J. Tranquanda for illuminating discussions.

[1] J. M. Tranquada, H. Woo, T. G. Perring, H. Goka, G. D. Gu, G. Xu, M. Fujita, and K. Yamada, Nature (London) **429**, 534 (2004).
[2] D. J. Scalapino and S. R. White, Phys. Rev. B **58**, 8222 (1998).
[3] E. Demler and S.-C. Zhang, Science **396**, 733 (1998).
[4] P. Dai, H. A. Mook, S. M. Hayden, G. Aeppli, T. G. Perring, R. D. Hunt, and F. Dogan, Science **284**, 1334 (1999).
[5] P. Dai, H. A. Mook, G. Aeppli, S. M. Hayden, and F. Dogan, Nature (London) **406**, 965 (2000).
[6] H.-Y. Kee, S. A. Kivelson, and G. Aeppli, Phys. Rev. Lett. **88**, 257002 (2002).
[7] G. Seibold and J. Lorenzana, Phys. Rev. Lett. **86**, 2605 (2001).
[8] G. Seibold, F. Becca, and J. Lorenzana, Phys. Rev. B **67**, 085108 (2003).
[9] G. Seibold, F. Becca, P. Rubin, and J. Lorenzana, Phys. Rev. B **69**, 155113 (2004).
[10] S. W. Lovesey, *Theory of Neutron Scattering from Condensed Matter* (Clarendon Press, Oxford, 1984).
[11] R. E. Walstedt and W. W. Warren, Jr., Science **248**, 1082 (1990).
[12] C. M. Canali, S. M. Girvin, and M. Wallin, Phys. Rev. B **45**, R10131 (1992).
[13] We neglect the small 7% variation of $Z_C(\boldsymbol{q})$ along the antiferro-

magnetic zone boundary predicted by Ref. 12 and R. R. P. Singh and M. P. Gelfand, Phys. Rev. B **52**, R15695 (1995); O. F. Syljuåsen and H. M. Rønnow, J. Phys.: Condens. Matter **12**, L405 (2000).

[14] R. R. P. Singh, Phys. Rev. B **39**, R9760 (1989).

[15] E. Manousakis, Rev. Mod. Phys. **63**, 1 (1991).

[16] I. U. Heilmann, J. K. Kjems, Y. Endoh, G. F. Reiter, G. Shirane, and R. J. Birgeneau, Phys. Rev. B **24**, 3939 (1981).

[17] T. Huberman, R. Coldea, R. A. Cowley, D. A. Tennant, R. L. Leheny, R. J. Christianson, and C. D. Frost, Phys. Rev. B **72**, 014413 (2005).

[18] C. M. Canali and M. Wallin, Phys. Rev. B **48**, 3264 (1993).

[19] A. W. Sandvik and R. R. P. Singh, Phys. Rev. Lett. **86**, 528 (2001).

[20] J. D. Perkins, J. M. Graybeal, M. A. Kastner, R. J. Birgeneau, J. P. Falck, and M. Greven, Phys. Rev. Lett. **71**, 1621 (1993).

[21] J. Lorenzana and G. A. Sawatzky, Phys. Rev. Lett. **74**, 1867 (1995).

[22] In the case of optical data the relevant operator is, to leading order, $S_i^x S_j^x + S_i^y S_j^y$ which involves Holstein-Primakoff bosons in nearest neighbor sites i and j, whereas in the case of neutron scattering longitudinal response the relevant operator is $\mathcal{N}_i$ which involves Holstein-Primakoff bosons on the same site. The associated response functions in the interacting case are reported in J. Lorenzana and G. A. Sawatzky, Phys. Rev. B **52**, 9576 (1995).

[23] M. A. Kastner, R. J. Birgeneau, G. Shirane, and Y. Endoh, Rev. Mod. Phys. **70**, 897 (1998).

[24] M. Grüninger, D. van der Marel, A. Damascelli, A. Erb, T. Nunner, and T. Kopp, Phys. Rev. B **62**, 12422 (2000).

[25] J. Lorenzana, J. Eroles, and S. Sorella, Phys. Rev. Lett. **83**, 5122 (1999).

[26] C. M. Canali and S. M. Girvin, Phys. Rev. B **45**, 7127 (1992).

[27] G. Fano, F. Ortolani, and A. Parola, Phys. Rev. B **42**, R6877 (1990).

[28] D. Vollhardt, Rev. Mod. Phys. **56**, 99 (1984).

[29] K. Yosida, *Theory of Magnetism* (Springer-Verlag, Berlin, 1996).

[30] R. Coldea, S. M. Hayden, G. Aeppli, T. G. Perring, C. D. Frost, T. E. Mason, S.-W. Cheong, and Z. Fisk, Phys. Rev. Lett. **86**, 5377 (2001).

[31] G. Seibold and J. Lorenzana, Phys. Rev. Lett. **94**, 107006 (2005).

[32] M. Roger and J. M. Delrieu, Phys. Rev. B **39**, 2299 (1989).

[33] H. J. Schmidt and Y. Kuramoto, Physica C **167**, 263 (1990).

[34] F. Lema, J. Eroles, C. D. Batista, and E. R. Gagliano, Phys. Rev. B **55**, 15295 (1997).

[35] G. Seibold and J. Lorenzana, Phys. Rev. B **69**, 134513 (2004).

[36] E. Pavarini, I. Dasgupta, T. Saha-Dasgupta, O. Jepsen, and O. K. Andersen, Phys. Rev. Lett. **87**, 047003 (2001).

[37] J. E. Hirsch and S. Tang, Phys. Rev. Lett. **62**, 591 (1989).

[38] S. B. Bacci, E. R. Gagliano, R. M. Martin, and J. F. Annett, Phys. Rev. B **44**, 7504 (1991).

[39] S. Uchida, T. Ido, H. Takagi, T. Arima, Y. Tokura, and S. Tajima, Phys. Rev. B **43**, 7942 (1991).

[40] H. M. Rønnow *et al.*, Phys. Rev. Lett. **87**, 037202 (2001).

[41] J. M. Tranquada, B. J. Sternlieb, J. D. Axe, Y. Nakamura, and S. Uchida, Nature (London) **375**, 561 (1995).

[42] S. Sachdev, *Quantum Phase Transitions* (Cambridge University Press, Cambridge, 2001).

[43] J. Lorenzana and L. Yu, Phys. Rev. Lett. **70**, 861 (1993).

[44] J. Lorenzana and G. Seibold, Phys. Rev. Lett. **90**, 066404 (2003).

[45] S. M. Hayden, G. Aeppli, H. A. Mook, T. G. Perring, T. E. Mason, S.-W. Cheong, and Z. Fisk, Phys. Rev. Lett. **76**, 1344 (1996).

[46] N. B. Christensen, D. F. McMorrow, H. M. Rønnow, B. Lake, S. M. Hayden, G. Aeppli, T. G. Perring, M. Mangkorntong, M. Nohara, and H. Tagaki, Phys. Rev. Lett. **93**, 147002 (2004).

[47] S. Wakimoto, H. Zhang, H. M. Rønnow, K. Yamada, I. Swainson, H. Kim, and R. J. Birgeneau, Phys. Rev. Lett. **92**, 217004 (2004).